Collaborative Mapping of an Earthquake-Damaged Building via Ground and Aerial Robots

Nathan Michael, Shaojie Shen, Kartik Mohta, Yash Mulgaonkar, and Vijay Kumar
GRASP Laboratory, University of Pennsylvania, Philadelphia, Pennsylvania 19104-3409
e-mail: nmichael@grasp.upenn.edu, shaojie@grasp.upenn.edu, kmohta@grasp.upenn.edu, yashm@grasp.upenn.edu, kumar@grasp.upenn.edu
Keiji Nagatani, Yoshito Okada, Seiga Kiribayashi, Kazuki Otake, Kazuya Yoshida, Kazunori Ohno, Eijiro Takeuchi, and Satoshi Tadokoro
Tohoku University, Sendai, Japan
e-mail: keiji@astro.mech.tohoku.ac.jp, okada@astro.mech.tohoku.ac.jp, seiga@astro.mech.tohoku.ac.jp, otake@astro.mech.tohoku.ac.jp, yoshida@astro.mech.tohoku.ac.jp, kazunori@rm.is.tohoku.ac.jp, takeuchi@rm.is.tohoku.ac.jp, tadokoro@rm.is.tohoku.ac.jp

Received 26 January 2012; accepted 27 June 2012

We report recent results from field experiments conducted with a team of ground and aerial robots engaged in the collaborative mapping of an earthquake-damaged building. The goal of the experimental exercise is the generation of three-dimensional maps that capture the layout of a multifloor environment. The experiments took place in the top three floors of a structurally compromised building at Tohoku University in Sendai, Japan that was damaged during the 2011 Tohoku earthquake. We provide details of the approach to the collaborative mapping and report results from the experiments in the form of maps generated by the individual robots and as a team. We conclude by discussing observations from the experiments and future research topics.

1. INTRODUCTION

In this work, we report recent results from field experiments conducted with a team of ground and aerial robots engaged in the mapping of an earthquake-damaged building. We focus on the investigation of the feasibility of deploying aerial robots, specifically a quadrotor, into disaster scenarios where a building may be critically damaged but is still accessible to robots and humans for experimental purposes. The experimental environment covered the top three floors of a building on the campus of Tohoku University in Sendai, Japan during the first week of August, 2011. Representative images of the interior and exterior of the building are shown in Figures 1 and 2.

On March 11, 2011, a magnitude 9.0 earthquake (on the moment magnitude scale) occurred off the coast of Japan, approximately 130 km from Sendai (USGS, 2011). The consequences of the earthquake were devastating, with significant loss of human life and damage to the environment. Resulting tsunami waves generated further damage and instigated a meltdown at a nuclear power plant near Fukushima, Japan (Tabushi, 2011).

Several robotics research groups and companies responded to this natural and nuclear plant disaster (Ackerman, 2011; Nagatani et al., 2011). Ground robots with onboard sensing enabled environmental observation of the compromised nuclear power plants in regions that were inaccessible to humans due to high levels of radioactivity. The ground robots were equipped with long-range cable tethers to enable remote communication, teleoperation, and the transmission of sensor data. These ground robots proved capable of maneuvering through the cluttered environments (Guizzo, 2011).

We are interested in exploring the possibility of leveraging an autonomous quadrotor in such environments through field experiments that focus on cooperative mapping using both ground and aerial robots. Aerial robots offer several advantages over ground robots, including the ability to maneuver through complex three-dimensional (3D) environments and gather data from vantages inaccessible to ground robots. Further, quadrotors are able to hover in place, making them well-suited for observation and human-guided or autonomous inspection. However, aerial robots also have several limitations that reduce their applicability in disaster scenarios. Such limitations include the need for wireless communication and a limited onboard power supply that restricts the platform's payload capacity and flying time.

Given the prior experience of using ground robots at the nuclear power plant disaster site, we designed the experimental scenario based on conditions consistent with those found at the disaster site. Consider an

Multimedia files may be found in the online version of this article.
This work builds upon the conference paper (Michael et al., 2012).
Direct correspondence to: Nathan Michael, e-mail: nmichael@seas.upenn.edu.

Figure 1. Panoramic images depicting the interior of the building. These images are representative of the clutter found throughout the experimental areas.

Figure 2. The building suffered significant structural damage due to the earthquake.

earthquake-damaged building with multiple floors that are generally accessible to ground robots. However, various locations in the environment are inaccessible to the ground robots due to debris or clutter. The goal of the experimental exercise is the generation of 3D maps that capture the layout of the environment and provide insight into the degree of damage inside the building. Additionally, there may be specific regions of interest that require attention from operators during the mapping. Throughout the experiments, remote operators must be able to maintain control of the robotics platforms on the ground and in the air.

The experiment design highlights the need for heterogeneity. Ground robots do not have the same payload limitations as quadrotors, and they are therefore able to carry larger sensor payloads, maintain tethered communication links, and operate for longer periods of time. However, quadrotors provide mobility and observational capabilities unavailable to ground robots. Hence, to build a rich 3D representation of the environment, we leverage the advantages of each platform, and in doing so we mitigate the platform limitations.

The problems of localization and mapping in 3D environments are well-studied for both ground and aerial robots, and many methodologies exist to address these problems. In this work, we focus primarily on the integration of our prior work in the areas of localization and mapping for ground and aerial robots. However, there are several examples of prior works employing methodologies similar to our own approach for either ground or aerial platforms (Bachrach et al., 2011; Pellenz et al., 2010), including cooperative mapping with ground and aerial platforms (How et al., 2009; Kim et al., 2010). Researchers have also pursued the mapping of complex environments for applications such as search and rescue via ground and aerial platforms (Gonzalez et al., 2011; Murphy et al., 2009; Pratt et al., 2008). Therefore, the contributions of this work are twofold. First, it supports experimentally the argument that the mapping of complex multistory environments with ground and aerial robots in disaster scenarios is viable (or nearly viable) given the current state-of-the-art in vehicle design, sensors, computation, and algorithms. Second, it supports the statement that the strengths and weaknesses of individual robot platforms may be overcome by employing heterogeneity in system design. Additionally, we provide a brief discussion of the gap between the current technological capabilities and the remaining challenges

we must overcome toward application in true disaster scenarios.

2. EXPERIMENT DESIGN AND METHODOLOGY

To address the requirements of the experimental scenario, we use three different research platforms. The first platform is a ground robot equipped with an onboard sensing suite that enables the generation of dense 3D maps. The vehicle is teleoperated through the multifloor environment while simultaneously collecting sensor data. After the operators identify locations in the environment that are inaccessible to the ground platform, a second ground platform equipped with an automated helipad is teleoperated to these locations and carries a quadrotor robot equipped with onboard sensing that is able to remotely open and close the helipad and autonomously take off and land from the helipad (Figure 3). The aerial robot is physically transported by the ground robot to each location of interest, where it autonomously takes off before an operator is able to guide the robot to map or observe these inaccessible regions. Upon completion of the mapping and observation phase, the aerial robot is remotely signaled to autonomously land and close the helipad. The quadrotor is then guided to the next location of interest via the teleoperated ground robot.

The experiment focuses primarily on the problems of localization and cooperative mapping in 3D environments with ground and aerial robots. In this work, we do not emphasize vehicle autonomy as the experiments required that the operators teleoperate the vehicles. We discuss this requirement further in Section 4. During the experiments, teleoperation is conducted over wireless communication. However, we assume that in a disaster scenario, the ground vehicles will communicate with an external operator via a tether as currently employed at the Fukushima site (Nagatani et al., 2011). Communications with the aerial robot are via a local access point carried by the ground robot.

Figure 3. The Quince ground platform carries the Pelican aerial robot via a landing pad. The aerial robot opens and closes the landing pad via a wireless interface during autonomous take off and landing. A video of the experiment is available as a multimedia attachment.

In this work, we leverage our previous efforts in the areas of ground robot design (Rohmer et al., 2010) sensor design for 3D map building (Ohno et al., 2008), and ground robot teleoperation (Okada et al., 2011) toward mapping with ground robots (Nagatani et al., 2008; Ohno et al., 2009; 2010). Additionally, we build upon prior work toward autonomous navigation and 3D mapping with an aerial robot (Shen et al., 2011; 2012).

2.1. Robot Platforms

As previously discussed, we employ three robot platforms for this work: two tracked ground platforms (Kenaf and Quince) and a quadrotor (Pelican). We now briefly detail each platform.

2.1.1. Ground Robots

The Kenaf is a tracked ground platform with an onboard rotating laser-scanner that provides feature-rich 3D point clouds of the environment (Figure 4(a)). The laser scanner on the Kenaf operates at 40 Hz and rotates about the vehicle body-frame at 0.2 Hz. All laser scans from one revolution are assembled into a 3D point-cloud aligned with the robot body-frame origin. Further details of the platform and 3D laser scanner are available in Ohno et al. (2009,2010) and Ohno et al. (2008), respectively. The Quince platform (detailed in Rohmer et al. (2010), Figure 4(b)) shares a similar tracked design. Both platforms provide odometry information and are equipped with stabilizing tracked arms that permit climbing stairs and navigating clutter- or debris-filled environments.

The Kenaf and Quince provide visual information for the teleoperation of the vehicle, including camera imagery of the surrounding environment during operation. We process any additional sensory information from the Kenaf and Quince offboard.

For this work, we equipped the Quince with a landing pad that opens and closes via a remote signal transmitted over an 802.15.4 wireless interface (Figure 4(c)). The landing platform is made of impact-resistant ABS plastic. The structural integrity is provided by an underlying framework of slotted aluminum extrusions. The arms that robustly grip the base of the aerial robot are also fabricated from ABS and lined with dense foam to provide additional compliance and absorb vibrational or impulse forces on the vehicle due to the Quince going over rough terrain and steps. Two pairs of aluminum carriage-rail assemblies ensure that the arms remain parallel to each other throughout the deployment and retraction phase. The gripping arms are driven by linear actuators and the motion of the two arms is governed by limit switches to prevent overextension or retraction. The onboard processor controls the direction and braking of the two linear actuators and receives control commands via the wireless interface.

(a) (b) (c)

Figure 4. The three robots used in the experiments include the Kenaf (a) and Quince (b) tracked ground robots. Here we see the Quince transporting the Pelican between discrete sites of interest via the landing pad (c).

Figure 5. The aerial robot flies through cluttered regions of the environment that are inaccessible to the ground robot and builds a 3D map that will be merged with the maps made by the ground robot.

2.1.2. Aerial Robot

The Pelican quadrotor robot platform is sold by Ascending Technologies, GmbH (Ascending Technologies, 2012) and is equipped with an IMU (accelerometer, gyroscope), magnetometer, and pressure sensor (Figure 5). We developed custom firmware to run at the embedded level to address feedback control and estimation requirements. The other computation unit onboard is a 1.6 GHz atom processor with 1 GB of RAM. The sensors on the robot include a Hokuyo UTM-30LX (laser) and a Microsoft Kinect (RGB-D sensor). A custom 3D printed mount is attached to the laser that houses mirrors pointing upward and downward. Communication with the robot for monitoring experiment progress and remote teleoperation is via an 802.11n access point mounted on the Quince.

Unlike the ground robots, the aerial robot requires some degree of onboard autonomy to permit autonomous navigation, takeoff, and landing. Therefore, the vehicle must be able to localize its position based on the current environment map and address the planning and control considerations required to permit autonomous navigation, takeoff, and landing during experimentation. The details of the algorithms employed to enable these capabilities are provided in Shen et al. (2011, 2012). Figure 9 depicts a representative 3D map generated online during the experiments that is transmitted to the operator and used for autonomous navigation.

For this work, we require some degree of operator control to permit teleoperation of the vehicle. However, the complexity of the environment and the fact that the operator frequently did not have line-of-sight vision of the vehicle prevented full manual control of the vehicle. Therefore, we provided a "semiautonomous" mode that permitted the operator to control the vehicle as a kinematic point-model agent or via waypoint control in the current map. Hence, at any moment, the operator could transition between full autonomy and semiautonomy to permit closer inspection of a location of interest or override the current behavior of the vehicle.

For this work, the autonomous takeoff and landing is based on the originating position of the aerial robot in the current map. Therefore, we required that the Quince not move while the Pelican was flying. Although the autonomous landing maneuver was feed-forward in the sense that it did not observe the platform while landing, we found that the vehicle was able to land without issue in general. However, the autonomous landing maneuver also included a recovery phase in the event that the vehicle detect that it did not successfully land on the platform. This lack of additional feedback information was due primarily to the short time frame in which these experiments needed

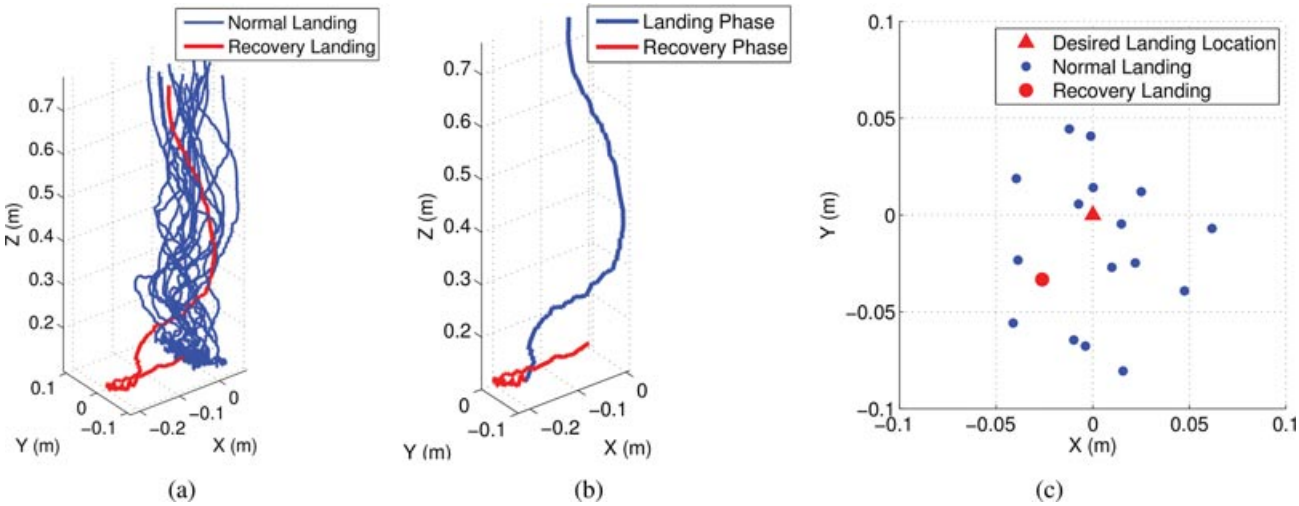

Figure 6. Partial trajectories of the aerial robot during 17 landing trials (a). During one trial, the vehicle attempts and fails to land, causing it to enter a recovery phase before successfully landing (b). A scatter plot of the final landing locations is shown in (c).

to be conducted prior to the experimental site becoming unavailable.

The recovery phase of the autonomous landing is based on the position of the robot with respect to the desired landing location. The primary source of error during landing is due to the ground effects induced by the vehicle's proximity to the landing pad. If the error between the desired landing location and the current vehicle state is within 2 cm in height but greater than 8 cm in either the x or y directions, the vehicle will enter a recovery phase in which it will attempt to regulate 1 cm above the desired landing location and concurrently estimate the changes in the dynamic model resulting from ground effects (as discussed in Shen et al. (2011)). The landing pad is designed to accommodate landing deviations of up to 10 cm in the x and y directions.

We evaluated the performance of the system to establish a suitable level of performance, both in landing pad design and autonomous flight, to permit operation in a feedforward manner as discussed above. Figure 6(a) depicts the performance of the vehicle over 17 trials in which the vehicle is asked to land autonomously from a variety of initial conditions, all an appreciable distance from the landing pad. Note that of these 17 trials, only one requires that the vehicle attempt to recover (Figure 6(b)). The intended and actual landing locations over the trials are shown in Figure 6(c).

2.2. Map Generation and Merging

We now briefly describe the methods used to generate the 3D maps during the experiment. The experiment consisted of two phases. During the first phase, we teleoperated the Kenaf across the three stories of the building and collected sensor data for 3D map generation. We also identified locations inaccessible to the vehicle (six in total). After completing the first mapping phase, the Quince carried the Pelican to the six locations across the three stories of the building to further extend the map. The maps are generated using a sparse 3D voxel grid representation with a 10 cm resolution (Dryanovski et al., 2010).

2.2.1. Kenaf

We used two methods to generate 3D maps via the Kenaf sensor data. The first approach uses a 3D iterative closest point (ICP) algorithm to determine incremental body-frame transformations. Details of map generation via this method are discussed in Ohno et al. (2009). However, as noted in our prior work, 3D ICP can converge to poor alignment solutions. We found that when the vehicle was operating on a level z-plane (i.e., not in a stairwell), we could yield a more robust mapping solution by employing the methods discussed in Shen et al. (2011), which requires the assumption that the environment is generally described by flat planes and vertical walls (the 2.5D assumption).

For this approach, map corrections are done on a per-revolution basis with the assumption that the odometry error within one revolution is sufficiently small and the assembled point-cloud is accurate. Error in yaw is also corrected using IMU information. Figure 7 shows a typical point-cloud output from one revolution. The point-cloud is down-sampled via a voxel grid filter, from which we generate a 2D point-cloud by choosing all samples at a fixed z-height. We compute SLAM corrections from this 2D point-cloud and odometry data via the methods detailed in Shen et al. (2011) to yield corrected robot poses. These corrected poses are used with the 3D point-clouds to

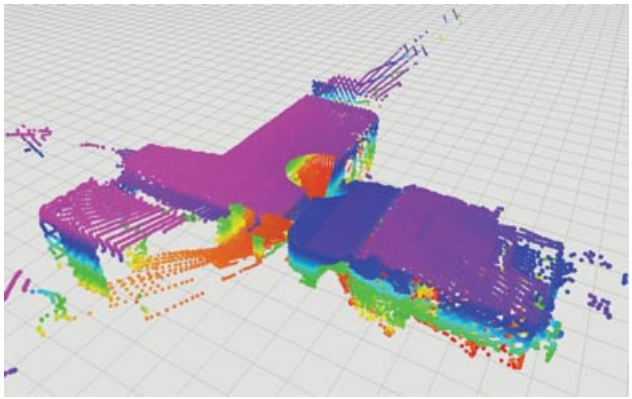

Figure 7. The 3D rotating laser scanner on the Kenaf generates feature-rich 3D point-clouds. Here we show the full output from a single revolution of the scanner.

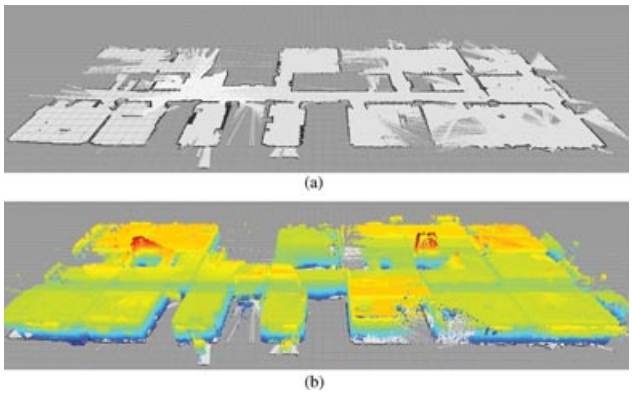

Figure 8. The 2D occupancy grid map (Figure 8(a)) and 3D point-cloud map (Figure 8(b)) of the 7th floor generated via the Kenaf sensor data.

generate globally consistent 3D maps of the environment (Figure 8(b)) along with 2D occupancy grid maps resulting from the 2.5D assumption (Figure 8(a)). In general, we applied the second method when operating on level terrain and only turned to the 3D ICP-based SLAM methods when operating in the stairwell regions.

2.2.2. Pelican

As previously noted the Pelican generates a 3D map online during autonomous flight following the methodology detailed in Shen et al. (2011). Unlike the Kenaf, the Pelican collects data at discrete locations in the environment with the origin associated with the takeoff location as visited by the Quince. In a manner similar to that mentioned above, we generate a 3D point-cloud and a 2D occupancy grid map associated with each takeoff location. Figure 9 depicts a representative visualization of the sensor data and generated maps. These maps are merged with the Kenaf maps from

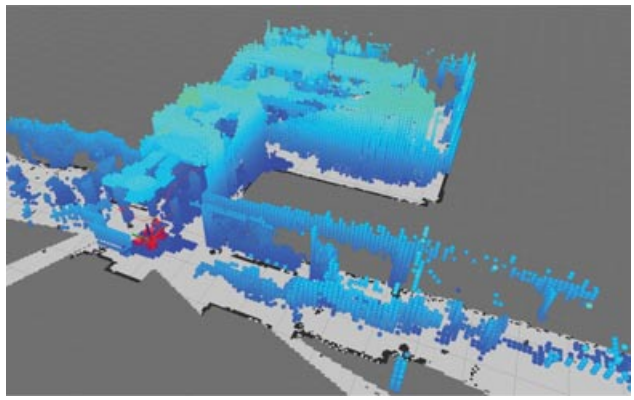

Figure 9. A representative 3D map generated by the aerial vehicle during flight. A 2D occupancy grid map is also generated at all times. The vehicle and its trajectory are shown as a red mesh and line, respectively.

the previous section to form a complete 3D representation of the environment.

2.2.3. Merging Ground and Aerial Robot Maps

We begin by registering the two types of maps (the Kenaf and Pelican maps) via an initialization point near the known takeoff location of the Pelican, as the Quince visits locations defined in the Kenaf map. Further refinement between the two maps is accomplished via ICP (Ohno et al., 2009,2010). This approach is applied for each of the rooms visited by the Pelican (Figure 10).

3. RESULTS

As previously noted, the goal of this work is the generation of 3D maps that capture the layout of the environment inside a multistory building. In Figures 11 and 12, we provide full 2D and 3D maps of the seventh through ninth floors of the building. We can clearly see features in the environment, such as the structural braces placed on the eighth floor (Figure 12(d)) to prevent further structural collapse, and the locations on the ninth floor (Figure 11(c)) where the walls caved out of the building, leaving large openings. In Figure 13, we show the 3D map for the stairwell between the seventh and eighth floors at various z-height levels.

The experiment lasted a total of 2.5 h with the Kenaf first generating a 3D map via teleoperation followed by the Quince carrying the Pelican to discrete locations (all starting on the seventh floor). It is worth noting that while the flight-time of the Pelican in confined environments can be as low as 5 min, we only needed to replace the battery in the vehicle twice due to the fact that we used the aerial robot only when necessary for map extension. Although our Pelican can traverse hallways and stairwells autonomously (as shown in Shen et al. (2011)), we conserved the battery

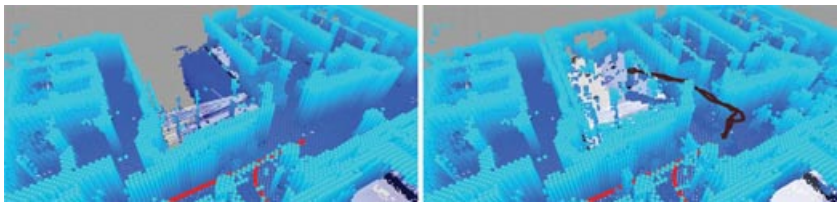

Figure 10. Merging the Kenaf and Pelican maps. The map generated by the Kenaf is shown on the left; the extended map via the Pelican observations along with the Quince and Pelican trajectories (red and black, respectively) is shown on the right.

Figure 11. The 2D occupancy grid maps generated during the experiment on the seventh, eighth, and ninth stories of the Tohoku University Electrical Engineering Building. The contributions to the map made by the Kenaf are shown in yellow with an overlay of the contributions made by the Pelican in green. The path of the Quince is shown in red while the trajectory followed by the Pelican is depicted in blue. The path of the Kenaf is not shown. The expected locations of walls based on structural blueprints are shown as gray lines. Several rooms could not be mapped due to operator safety concerns. Two rooms could not be mapped due to ground robot inaccessibility and violation of the 2.5D assumption.

power whenever possible by employing the Quince. For this work, the Pelican is equipped with a continuous power supply circuit that permits manual online hot-swapping of batteries by the operator. However, we are currently pursuing a system design that enables online battery recharging while the vehicle is docked on the landing pad.

4. DISCUSSION, CONCLUSION, AND AREAS FOR FUTURE WORK

The original experiments were intended to occur over several days, but we found that we were able to complete the full exercise in one afternoon without any failures. The fact that we were able to map a multistory building with a heterogeneous team of robots without any significant issues or failures is an encouraging argument that the technological readiness level of such methods is moving toward applicability in real scenarios. However, there are still some fundamental challenges left to address.

We must first acknowledge that the environment was modified prior to our entry in that it was cleaned of any hazardous materials and structural reinforcements were put into place to prevent further building collapse. For this reason, one should be cautious to state that our experiments are completely representative of an earthquake-damaged building. However, the environment still possessed similar attributes to what one would expect: fallen beams, dust and debris throughout the interior, water pools where rain freely entered the building, wires hanging from the ceiling, and personal affects and furniture in disarray. Indeed, loose wall and ceiling materials were of concern for both the ground and aerial robots due to the possibility that such material could damage the vehicles. Many of the windows and walls were compromised, yielding inconsistent air flow that impacted the aerial robot's flight performance. Additionally, some of the debris and clutter proved to test the 2.5D assumption employed by the aerial robot to simplify the localization problem and permit real-time performance. Hence, we were not able to use the aerial robot in all locations that were inaccessible to the ground robot (see Figure 11).

The 3D voxel grid-based maps resulting from this work provide insight into the building layout and structural information, but they may be too coarse to be of practical use in real search-and-rescue applications. Recent progress in the area of dense 3D mapping suggests that high-fidelity maps suitable for real search-and-rescue applications are achievable using laser and RGB-D sensors (Ellekilde et al., 2007; Huang et al., 2011). Further, these richer 3D maps can be generated offline or on an external system as they are not required to enable individual vehicle autonomy. Thus, the major constraint is the communication

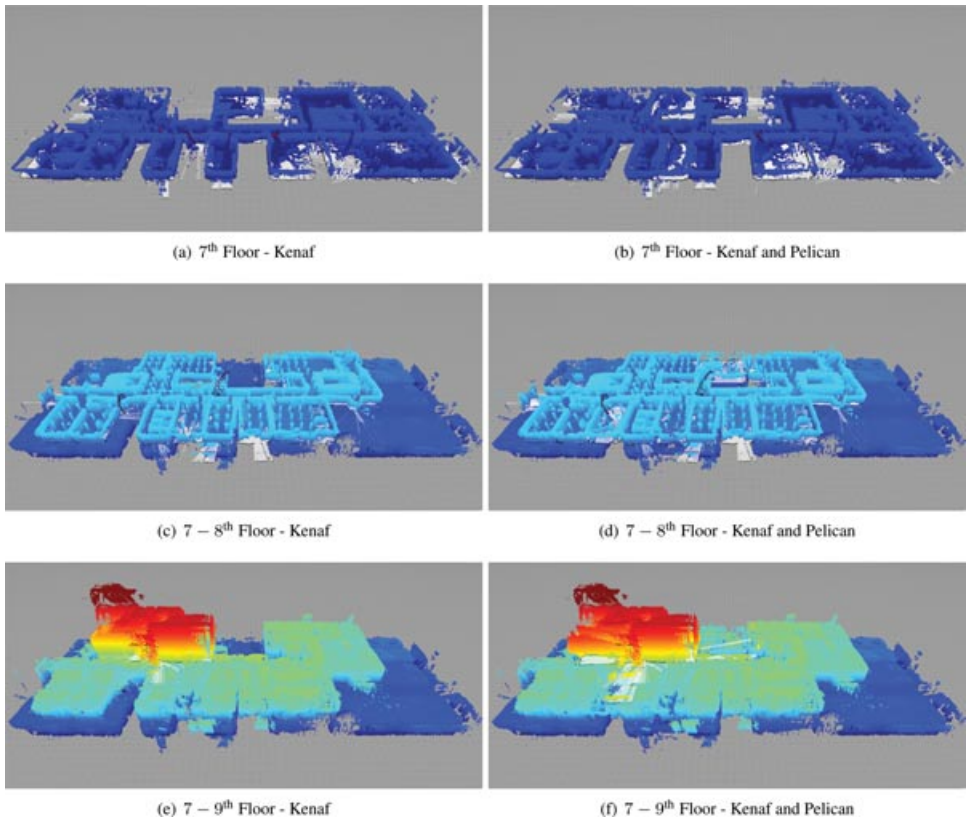

Figure 12. The 3D voxel grid maps generated during the experiment. The map resulting from the Kenaf sensor data is shown on the left, the merged maps resulting from both the Kenaf and Pelican sensor data are shown on the right.

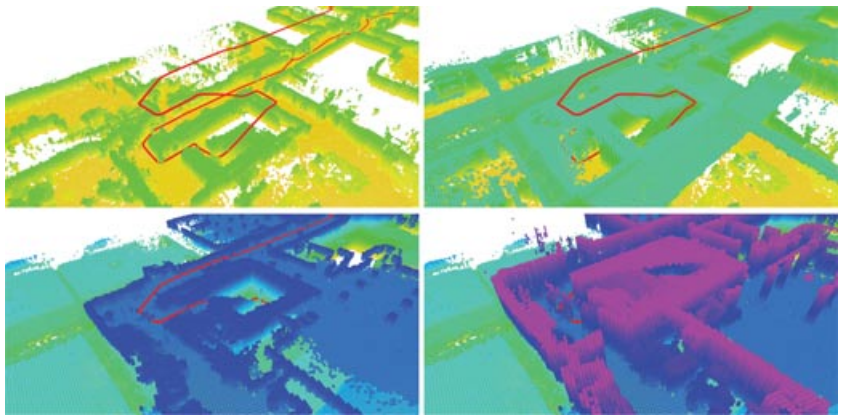

Figure 13. The 3D map generated for the stairwell traversed by the vehicles between the seventh and eighth floors showing various z-height levels of detail along with the trajectory followed by the Quince robot.

bandwidth required to transfer the data between aerial and ground vehicles and the base station. In this work, we consider a tethered ground robot with an aerial vehicle operating in close proximity communicating via 802.11n. Therefore, we believe that given the proposed heterogeneous team, such rich 3D maps are feasible following the implementation methods proposed in Ellekilde et al. (2007) and Huang et al. (2011).

In addition to the platform or algorithmic limitations, an interesting consideration that arose in this work is the role of autonomy for aerial robots in search and rescue. We found that teleoperation of an aerial robot can be quite

challenging in complex and confined environments, particularly when the operator does not have direct line-of-sight and debris is interacting with the vehicle. An autonomous vehicle may be able to sense and locally avoid those external interactions and preserve stable flight, whereas a teleoperated system may not yield the same result. We found this to be the case at several points during our experimentation when the operator failed to navigate the vehicle through tightly confined spaces, but the fully autonomous vehicle was able to find a path and navigate autonomously through the confined space.

From these statements, one may conclude that for search-and-rescue missions, the areas that require the greatest attention in the future do not lie in the core problems of localization and mapping but more at the boundaries of these problems, including the interfaces between the operators and the vehicles and the vehicles and the environment. We require a better understanding of the appropriate methods to permit operators to interact with aerial robots in complex and confined environments such as those found in this work. Additionally, we must design aerial vehicles to be more robust to debris in the environment. In this work, we did not notice a significant impact on sensor performance (laser and RGB-D) due to dust or other airborne obscurants. However, this is likely due to the nature of the building airflow conditions rather than the sensor robustness as this is a known concern (Sevcik et al., 2010), and it should therefore also be considered when determining platform suitability for real applications.

While there are still issues that must be addressed in the algorithms, these problems are primarily of pragmatic concern. At present, we require the 2.5D assumption on the aerial vehicle due to constrained onboard CPU capabilities. As CPUs become increasingly capable, we will continue to incorporate more sensor information and eliminate the need for the 2.5D assumption. We are particularly interested in eliminating this assumption in the near future as it is a major algorithmic limitation for the aerial platform. We are also interested in further experimentation with cooperative teams of ground and aerial robots but with multiple ground and aerial robots operating concurrently as opposed to the sequential phases in this work.

5. APPENDIX: INDEX TO MULTIMEDIA EXTENSIONS

The video is available as Supporting Information in the online version of this article.

Extension	Media Type	Description
1	Video	Experimental results reported in the paper.

ACKNOWLEDGMENTS

The authors gratefully acknowledge partial support from NSF Grant CNS-1138110, ARL Grant W911NF-08-2-0004, the JST J-RAPID program, and the NEDO Project for Strategic Development of Advanced Robotics Elemental Technologies.

REFERENCES

Ackerman, E. (2011). Japan earthquake: iRobot sending Packbots and Warriors to Fukushima Dai-1 nuclear plant. In IEEE Spectrum. Source: http://spectrum.ieee.org/automaton/robotics/industrial-robots/irobot-sending-packbots-and-warriors-to-fukushima.

Ascending Technologies (2012). Ascending Technologies, GmbH. Retrieved May 29, 2012, from http://www.asctec.de.

Bachrach, A., Prentice, S., He, R., & Roy, N. (2011). RANGE - robust autonomous navigation in GPS-denied environments. Journal of Field Robotics, 28(5), 644–666.

Dryanovski, I., Morris, W., & Jizhong, X. (2010). Multi-volume occupancy grids: An efficient probabilistic 3D mapping model for micro aerial vehicles. In Proc. of the IEEE/RSJ Intl. Conf. on Intell. Robots and Syst. (pp. 1553–1559), Taipei, Taiwan.

Ellekilde, L.-P., Huang, S., Miro, J. V., & Dissanayake, G. (2007). Dense 3D map construction for indoor search and rescue. Journal of Field Robotics, 24(1-2), 71–89.

Gonzalez, F., Castro, M. P. G., Narayan, P., Walker, R., & Zeller, L. (2011). Development of an autonomous unmanned aerial system to collect time-stamped samples from the atmosphere and localize potential pathogen sources. Journal of Field Robotics, 28(6), 961–976.

Guizzo, E. (2011). Fukushima robot operator writes tell-all blog. In IEEE Spectrum. Source: http://spectrum.ieee.org/automaton/robotics/industrial-robots/fukushima-robot-operator-diaries.

How, J. P., Fraser, C., Kulling, K. C., Bertuccelli, L. F., Toupet, O., Brunet, L., Bachrach, A., & Roy, N. (2009). Increasing autonomy of UAVs. IEEE Robotics and Automation Magazine, 16(2), 43–51.

Huang, A. S., Bachrach, A., Henry, P., Krainin, M., Maturana, D., Fox, D., & Roy, N. (2011). Visual odometry and mapping for autonomous flight using an RGB-D camera. In Proc. of the Intl. Symp. of Robot. Research, Flagstaff, AZ.

Kim, B., Kaess, M., Fletcher, L., Leonard, J., Bachrach, A., Roy, N., & Teller, S. (2010). Multiple relative pose graphs for robust cooperative mapping. In Proc. of the IEEE Intl. Conf. on Robot. and Autom. (pp. 3185–3192), Anchorage, AK.

Michael, N., Shen, S., Mohta, K., Kumar, V., Nagatani, K., Okada, Y., Kiribayashi, S., Otake, K., Yoshida, K., Ohno, K., Takeuchi, E., & Tadokoro, S. (2012). Collaborative mapping of an earthquake-damaged building via ground and aerial robots. In Proc. of the Intl. Conf. on Field and Service Robot., Matsushima, Japan.

Murphy, R., Kravitz, J., Stover, S., & Shoureshi, R. (2009). Mobile robot in mine rescue and recovery. IEEE Robotics and Automation Magazine, 16(2), 91–103.

Nagatani, K., Kiribayashi, S., Okada, Y., Tadokoro, S., Nishimura, T., Yoshida, T., Koyanagi, E., & Hada, Y. (2011). Redesign of rescue mobile robot Quince - toward emergency response to the nuclear accident at Fukushima Daiichi nuclear power station on March 2011. In Proc. of IEEE Intl. Symp. on Safety, Security, and Rescue Robotics (pp. 13–18), Kyoto, Japan.

Nagatani, K., Tokunaga, N., Okada, Y., & Yoshida, K. (2008). Continuous acquisition of three-dimensional environment information for tracked vehicles on uneven terrain. In Proc. of the IEEE Intl. Workshop on Safety, Security, and Rescue Robot., Sendai, Japan.

Ohno, K., Kawahara, T., & Tadokoro, S. (2008). Development of a 3D laser scanner for measuring uniform and dense 3D shapes of static objects in dynamic environments. In Proc. of IEEE Intl. Conf. on Robot. and Biomimetics (pp. 2161–2167), Bangkok, Thailand.

Ohno, K., Tadokoro, S., Nagatani, K., Koyanagi, E., & Yoshida, T. (2009). 3-D mapping of an underground mall using a tracked vehicle with four sub-tracks. In IEEE Intl. Workshop on Safety, Security, and Rescue Robotics, Denver, CO.

Ohno, K., Tadokoro, S., Nagatani, K., Koyanagi, E., & Yoshida, T. (2010). Trials of 3-D map construction using the teleoperated tracked vehicle Kenaf at Disaster City. In Proc. of the IEEE Intl. Conf. on Robot. and Autom. (pp. 2864–2870), Anchorage, AK.

Okada, Y., Nagatani, K., Yoshida, K., Tadokoro, S., Yoshida, T., & Koyanagi, E. (2011). Shared autonomy system for tracked vehicles on rough terrain based on continuous three-dimensional terrain scanning. Journal of Field Robotics, 28(6), 875–893.

Pellenz, J., Lang, D., Neuhaus, F., & Paulus, D. (2010). Real-time 3D mapping of rough terrain: A field report from Disaster City. In Proc. of the IEEE Intl. Workshop on Safety, Security, and Rescue Robot., Bremen, Germany.

Pratt, K. S., Murphy, R. R., Burke, J. L., Craighead, J., Griffin, C., & Stover, S. (2008). Use of tethered small unmanned aerial system at Berkman Plaza II collapse. In Proc. of the IEEE Intl. Workshop on Safety, Security, and Rescue Robot., Sendai, Japan.

Rohmer, E., Yoshida, T., Ohno, K., Nagatani, K., Tadokoro, S., & Koyanagi, E. (2010). Quince: A collaborative mobile robotic platform for rescue robots research and development. In Intl. Conf. on Adv. Mechatronics (pp. 225–230), Osaka, Japan.

Sevcik, K. W., Kuntz, N., & Oh, P. Y. (2010). Exploring the effect of obscurants on safe landing zone indentification. Journal of Intelligent and Robotic Systems, 57(1-4), 281–295.

Shen, S., Michael, N., & Kumar, V. (2011). Autonomous multi-floor indoor navigation with a computationally constrained MAV. In Proc. of the IEEE Intl. Conf. on Robot. and Autom. (pp. 20–25), Shanghai, China.

Shen, S., Michael, N., & Kumar, V. (2012). Autonomous indoor 3D exploration with a micro-aerial vehicle. In Proc. of the IEEE Intl. Conf. on Robot. and Autom. (pp. 9–15), Saint Paul, MN.

Tabushi, H. (2011). Company believes 3 reactors melted down in Japan. In The New York Times. Source: http://www.nytimes.com/2011/05/25/world/asia/25nuclear.html.

USGS (2011). Magnitude 9.0 - near the east coast of Honshu, Japan. In U.S. Geological Survey. Source: http://earthquake.usgs.gov/earthquakes/eqinthenews/2011/usc0001xgp.